5th International Conference on Experimental Fluid Mechanics ICEFM 2018 Munich
Munich, Germany, July 2-4, 2018

Coherent structures within the laminar separation bubble on a NACA 0015 hydrofoil

Massimo Miozzi[1*], Alessandro Capone[1], Marco Costantini[2], Christian Klein[2], Fabio Di Felice[1]

[1] CNR-INM (formerly INSEAN),Marine Technology Institute of National Research Council / Rome / Italy

[2] DLR (German Aerospace Center) / Göttingen / Germany

[*] massimo.miozzi@cnr.it

Abstract

We report about the topology and the coherent structures inside the recirculating region of the Laminar Separation Bubble (LSB) that appear on the suction side of a NACA 0015 hydrofoil at Angles of Attack $AoA = [3^\circ, 10^\circ]$ and at chord Reynolds number $Re = 1.8 \times 10^5$. The non-intrusive Temperature Sensitive Paint (TSP) technique provides the thermal footprints $T_w(x,y,t)$ of the fluid on the model surface, unveiling three different flow regimes whose complexity in time and space decreases when AoA increases. $T_w(x,y,t)$ maps are analyzed by applying an optical-flow-based method to extract the relative skin-friction fields; the obtained τ_w lines provide a topological description of the flow at the wall. The analysis of the critical points shows that, with a fair level of generality, the separation region $\mathfrak{S}$ is composed by a sequence of manifolds which connect saddle points to converging nodes via the saddles unstable manifolds whereas, in a complementary way, the reattachment region $\mathfrak{R}$ is composed by a sequence of manifolds which connect saddle points to converging nodes via the saddles stable manifolds. This ubiquitous configuration is common to both the examined AoA and represents an essential portrait of the investigated LSB structure which fully agrees with 3D separation theory. 2D and 3D disturbances strongly alter this scenario. In the paper we report about:

- the extraction of the τ_w vector fields after the application of the optical-flow based algorithm;
- the evolution of the flow topology at separation $\mathfrak{S}$ at $AoA = [3^\circ, 10^\circ]$ and reattachment $\mathfrak{R}$ at $AoA = 10^\circ$;
- the effect of weak 2D and 3D disturbances on the topology of the LSB at $AoA = 10^\circ$

1 Introduction

Experiments have been carried out in the cavitation tunnel CEIMM at CNR-INM (formerly INSEAN) on the suction side of a NACA 0015 hydrofoil model by means of Temperature Sensitive Paint (TSP). The investigations here reported have been conducted at angles of attack $AoA = [3^\circ, 10^\circ]$ and at $Re = 1.8 \times 10^5$. A region of recirculating flow was identified confined between laminar separation and turbulent reattachment lines. This region is commonly referred to as Laminar Separation Bubble (LSB) and has been the subject of many numerical and experimental investigations because of its impact on the efficiency of lifting air/hydro foils, especially at low Reynolds numbers (see Burgmann and Schröder (2008) and references within). The non-intrusive TSP approach allows for a description of the flow interaction with the body surface exactly at the wall avoiding any appreciable flow perturbation or wall property modification (see Tropea et al. (2007)). The extracted TSP maps (see Liu and Sullivan (2005) for a description of the standard setup) retain a detailed portrait of the footprints of the coherent flow structures that flush against the surface. Under the hypothesis that the wall heat flux is mainly due to the convective action of the flow, Liu and Woodiga (2011) proposed a systematic method for extracting skin-friction vector fields from single TSP images grounded on the asymptotic expression of the energy equation at wall. The skin-friction lines within those vector fields provide a topological description of the flow at the wall that minimizes the redundancy in describing the complex interactions of flow structures by addressing the nature of the critical points in the vector field

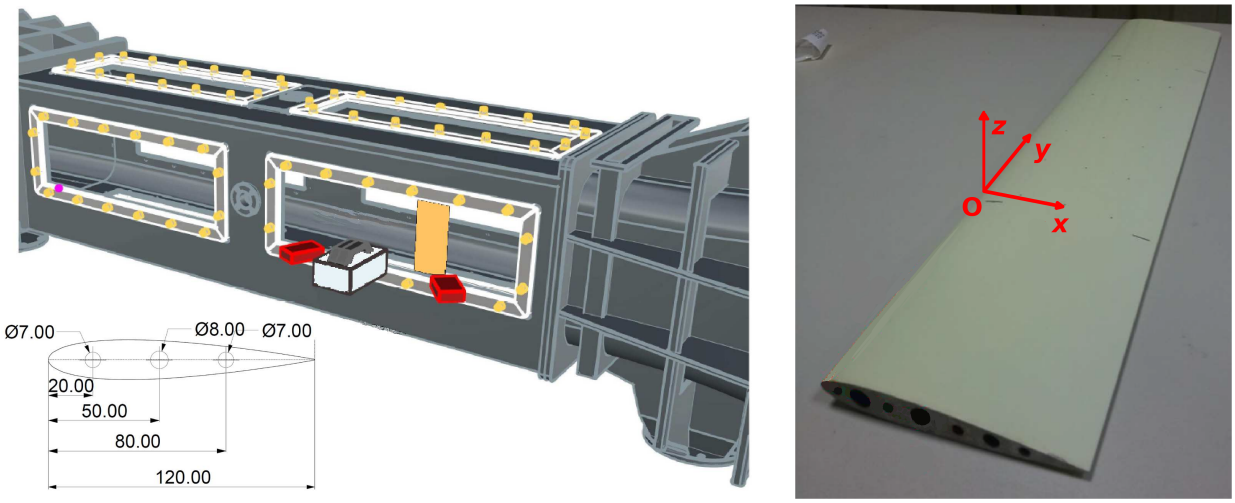

(a) CEIMM tunnel (b) TSP coated profile

Figure 1: (a) Water tunnel experimental setup and NACA 0015 hydrofoil model (orange, inside the tunnel), LED (red) and fast camera (white). Lower left detail reports the NACA 0015 profile with heating structure (distances in mm). (b) TSP-coated hydrofoil model. Registration markers can be noticed onto the surface. Reference coordinates given.

itself (see Miozzi et al. (2016)). In other words, their topology provide, via the critical lines and points, a simplified, essential skeleton which still allows a full understanding of the nature of the flow. In this work the focus is placed on the topology of the coherent structures that appear in the reverse flow inside the recirculating region at different AoA. Following Surana et al. (2006), here the separation line $\mathfrak{S}$ is identified as the composition of manifolds at the wall that move from a saddle point (S_i) to converging nodes (N_i,N_{i+1}) via the saddle unstable manifold. In a complementary way, the reattachment location $\mathfrak{R}$ is composed of a sequence of manifolds moving from diverging nodes to saddle points via the saddle stable manifold. Stable (converging) manifolds of saddle points S mark regions of weakly impinging flow (lower temperature) while nodes N are separation points of maxima of T'_w. The alteration of this ubiquitous arrangement at $AoA = 10^\circ$ by weak 2D and 3D instabilities give rise to more complex, but still readable, topology configurations and are reported in Sec. 3.

2 Experimental setup

The cavitation tunnel CEIMM consists of a closed-loop water tunnel featuring a $1:5.96$ contraction nozzle and a square test section of side $B = 600\,\text{mm}$. Free-stream turbulence intensity and flow uniformity at the channel centerline are respectively 0.6% at hydrofoil position (1.5% on average in the test section) and 1%. The test section is bounded by perspex windows in order to allow optical access from all directions. The hydrofoil model cross-section is a NACA 0015, chord length $C = 120\,\text{mm}$ and model span width L equal to test section side B. The model was coated with a temperature-sensitive paint (TSP) to measure the surface temperature. The development and the properties of the TSP used in this work are described in Ondrus et al. (2015). The hydrofoil model, as shown in Fig. 1(b), is mounted at the channel centerline by means of two flanges which can be rotated to set the desired angle of attack. The images were acquired by a CMOS high-speed camera Photron Fastcam SAX, 1024 square pixels resolution, fitted with a Nikon 50 mm focal length lens with 1.4 maximum aperture and a long-wave pass filter having a 50% transmittance cut-point at 600 nm wave length. TSP coating excitation light is provided by twelve high-power LEDs, having their maxima in the wavelength range between 400 nm and 405 nm. Acquisitions were carried out at free-stream velocity $U = 1.5\,\text{m/s}$, corresponding to Reynolds number $Re = 1.8 \times 10^5$ based on the chord length, and at angle of attack $AoA = 3^\circ$ and 10°. A sets of $10,916$ images was collected with acquisition frequencies of $F = 1\,\text{kHz}$. Imaged area for all acquisitions was approximately $135 \times 135\ mm^2$, thus image spatial resolution was $\approx 0.13\,\text{mm/pixel}$. In order to establish a heat flux between the hydrofoil model surface and water, a temperature gradient has to be artificially created between the model profile and the surrounding fluid. To

this aim the hydrofoil model was manufactured with three internal circular cavities having different diameters (7, 8 and 7 mm, positioned respectively at 20, 50 and 80 mm from the leading edge, see Fig. 1(a) (detail at lower left), through which warm water flows. This is supplied by an external thermostatic bath which keeps the inner-fluid temperature constant at a target value, about 15° higher than the free stream temperature T_∞. After reached, the target temperature was kept by the thermostatic bath for a long time (more than 5 min) before the experiment started. Then, the short duration of the tests (10 s) allows to consider the target temperature as a constant in that time lapse.
In order to assess whether natural convection plays a role, the Richardson non-dimensional number is calculated as:

$$Ri = (g\beta(T_w - T_\infty)C)/U^2 \tag{1}$$

which represents the importance of natural convection relative to forced convection with β representing the volumetric thermal expansion coefficient and T_w the hydrofoil model surface temperature. Typically, it is assumed that natural convection is negligible for $Ri < 0.1$. At the tested Reynolds number and angles of attack $Ri < 0.001$ holds and consequently natural convection can be reasonably deemed negligible.

2.1 Pre-processing methods

2.1.1 Temperature maps extraction

The acquired images were pre-processed according to the common practice adopted generally when dealing with TSP acquisitions. A detailed description can be found in Fey et al. (2003) and Capone et al. (2015). The aim of the procedure is to minimize the effect of non-uniform illumination, uneven coating and non-homogeneous luminophore concentration in the TSP active layer (Liu and Sullivan (2005)). In the presented experiments the hydrofoil model underwent a certain amount of displacement due to lift, this causing the reference and run images to mismatch. An image re-alignment step (image registration) was then necessary prior to the pixel-wise ratio calculation step. Based on reference markers printed onto the TSP coating, visible in Fig. 1(b), an affine geometric transformation was thus employed to re-align images. The ratioed images were converted to thermal maps by using an appropriate calibration curve (Capone et al. (2015)).

2.1.2 Spatial filtering

Although uneven paint coating and nonuniform surface illumination can be significantly reduced by following the procedure described in Sec. 2.1.1, TSP images are still affected by a signification amount of Gaussian, additive, white noise and a filtering is strongly suggested. With the aim to improve the efficiency of the classical Gaussian filter, an edge-preserving spatial filtering was developed in order to enhance the relevant image gradients in TSP images, while removing the background, uncorrelated noise. The proposed filter is an enhanced version of the classical Gaussian blur: a circular Gaussian kernel is applied to the image where where the luminosity gradients are negligible, whereas a weakly stretched Gaussian kernel in the direction normal to the gradient itself is applied to the image where it exhibits a spatially coherent gradient, thus preserving the gradient itself from smoothing (see Miozzi et al. (2018)).

2.1.3 Temporal filtering

Data are filtered in time with a Savitzky-Golay filter. It can be thought as a generalized moving average, which approximates the underlying function within the moving window by a polynomial of higher order. The filter was applied to each pixel's luminosity time series, with a polynomial order of 1 and a span of $2M + 1 = 13$, where M is the impulse-response half length Schafer (2011). This corresponds to a nominal normalized cutoff frequency $f_{nc} = 0.165$ (Schafer (2011)), where the transfer function is 3 dB. The dimensional cutoff frequency of the filtered dataset is $f_c = 0.5 \times 0.165 \times 1000 = 82.5$ Hz.

2.2 Relative skin-friction via optical flow analogy

The Taylor expansions of the velocity and temperature fields close to a wall that bounds the flow field allows one to gain the asymptotic form of the energy equation as

$$F + \tau_{w_i} \frac{\partial T_w}{\partial X_i} = 0 \tag{2}$$

where T_w is the wall temperature, $\tau_{w_i} = \mu(\frac{\partial u_i}{\partial z})_w$ are the skin-friction components and F is a source term containing the time rate of heat flux, the thermal diffusion and the viscous dissipation contributions (Liu and Woodiga (2011)). Eq. 2 provides a relation between skin-friction vector, heat flux and temperature gradients at the wall. It represents a balance between the skin-friction vector projected on the normal vector ∇T_w to an isotemperature line $T_w = const$. The skin-fiction vector $\tau_w(x,y,t)$ can be extracted by solving the ill-posed problem represented by Eq. 2 with an inverse procedure by following a variational approach, to gain the relative estimation of τ_w at wall.

2.2.1 Low and high spatial wave-number decomposition for temperature maps visualization

With the aim to provide a more understandable visual description of the fluctuating temperature map T'_w, a low/high wave-number decomposition is applied to T_w by simply subtracting a Gaussian blurred image from the original one. The kernel adopted to generate the blurred image has a dimension D twice the larger structure inside the original image and a standard deviation of $D/2$.

3 Coherent structures inside LSB

A detail of the high wave-number instantaneous temperature map T'_w at $AoA = 10^\circ$ that includes both $\mathfrak{S}$ and $\mathfrak{R}$ is reported in Fig. 2(a), while Fig. 2(b) shows a detail of T'_w at $AoA = 3^\circ$ that includes $\mathfrak{S}$. Both maps have overlapped their wall shear stress τ_w lines with the same topological structure. As a matter of fact, at both flow conditions one can observe an horizontal strip of higher temperature which separates two regions having opposite velocities. In correspondence to this warmer strip, saddle points of τ_w lines are connected to converging nodes via the saddle points unstable manifolds. The converging nodes are *loci* of separation (Délery (2013)) whose temperature is higher than the temperature of the connected saddle points, because the unstable manifold marks the existence of a weak, impinging, cooler flow (see Miozzi et al. (2016) for a detailed description). Moreover, the complementary structure of $\mathfrak{R}$ in Fig. 2(a) can be described as a set of manifolds which connect diverging nodes to saddle points, via the stable manifolds of the saddle points. Although less evident than for $\mathfrak{S}$, a temperature gap between nodes and saddles is still observed because diverging nodes are *loci* of flow impingement and the fresh fluid from outside decrease their temperature more efficiently than for the saddle points. The configurations here described for both $\mathfrak{S}$ and $\mathfrak{R}$ fullfil the *Criteria S2 and R2* reported in Surana et al. (2006) for a separation and reattachment line respectively. At $AoA = 10^\circ$, the spatial arrangement of the LSB allows to define a rigid separation between the incoming, laminar flow, the reverse flow within the LSB and the turbulent flow after reattachment. This scenario is intermittently smeared by the raising of 2D and 3D disturbances that alter the structure of the flow topology, as shown in Fig. 3. The snapshot of T'_w here reported shows a 2D disturbance on the left (left rectangle on top, left detail bottom), probably due to the temporary collapse of the *dead-water* region, which strongly displaces the separation line towards the trailing edge. Simultaneously, an isotropic node appears (right rectangle on top, right detail on bottom), which marks the raising of a new structure, identifiable as a toroidal vortex, leading to the impingement of fresh fluid towards the wall.

4 Conclusion

The topological description of the separation region at $AoA = 3^\circ$ and 10° given in Fig. 2(a), 2(b) and 3 provide a syntesis for the description of the actual separation line $\mathfrak{S}$ which agrees with the requirements reported in *Criterion S2* in Surana et al. (2006), i.e. it moves from a saddle point and join a stable node through the unstable saddle manifold. Here we suppose that the requirement of *strong S-hyperbolicity* of $\mathfrak{S}$ can be satisfied because of the continuity of the τ curvature around $\mathfrak{S}$ itself. It can be noticed that the same τ topology can be identified from $AoA = 3^\circ$ up to $AoA = 10^\circ$. Figs. 2(a) and 2(b) report the position of two saddle points along $\mathfrak{S}$ connected, through their unstable manifold, to a set of converging nodes via their unstable manifolds. These manifolds are part of a long, irregular sequence of concatenating *C*-shaped elements, whose curvature decreases with increasing *AoA*. At the same time, Fig. 2(a) reports saddle points along $\mathfrak{R}$ connected to diverging nodes which are part of a long, irregular sequence of concatenating manifolds that define the reattachment location and fulfills the requirements reported in *Criterion R2* in Surana et al. (2006).

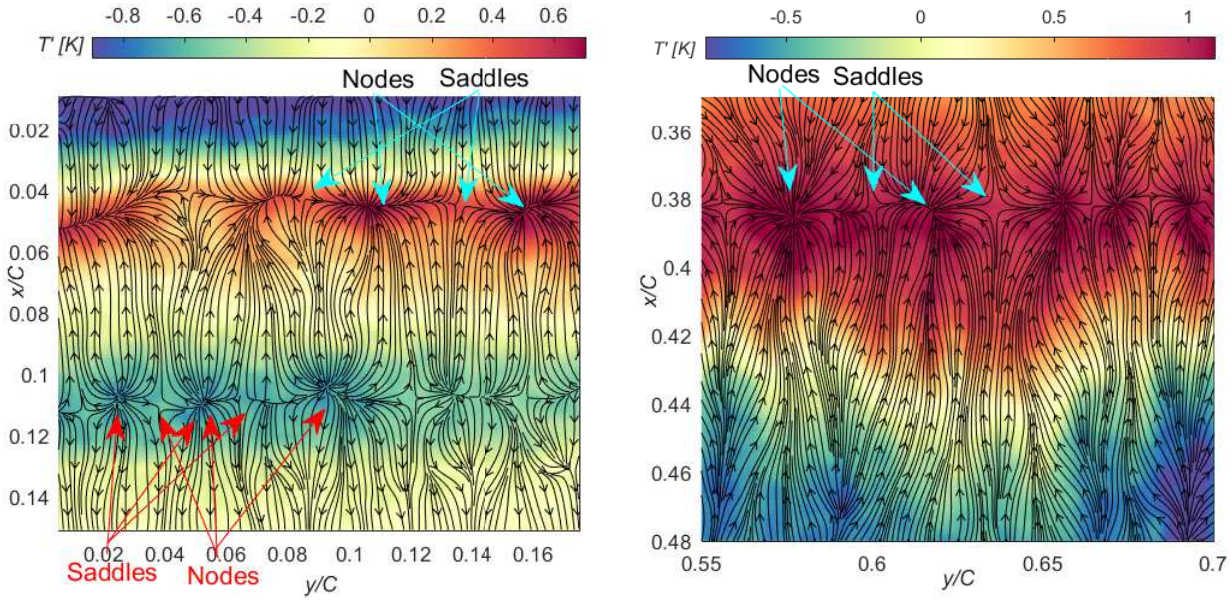

(a) Flow topology at $AoA = 10°$

(b) Flow topology at $AoA = 3°$

Figure 2: High wave-number component T'_w at $AoA = 10°$ (a) and $AoA = 3°$ (b). In the reverse flow region, inside the LSB, the sweep of cold fluid blobs from the outer flow push upstream against the warmer areas towards the leading edge. The saddle points and nodes which appear in the strip between the two regions fulfill the *Criterion S2* reported in Surana et al. (2006) for a separation line.

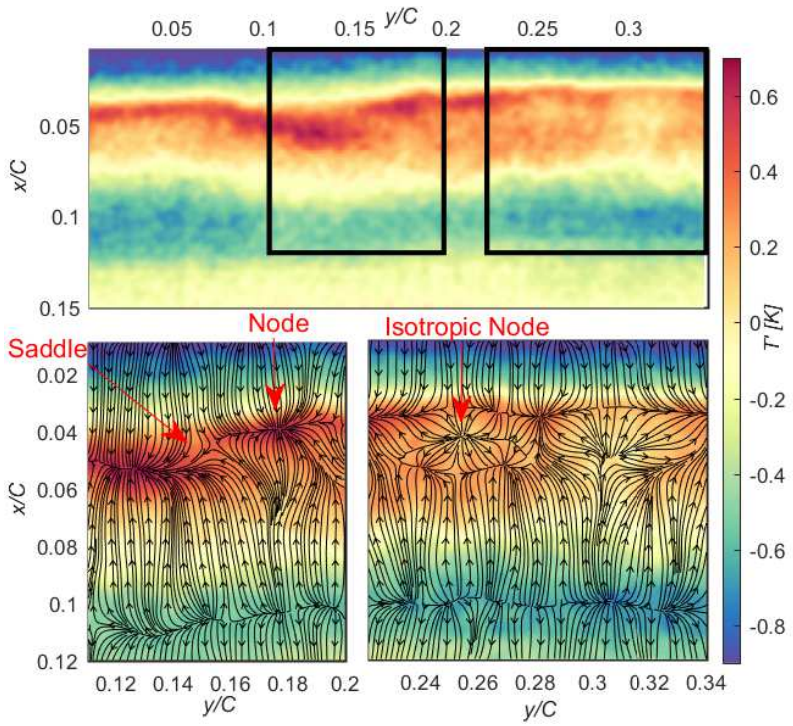

Figure 3: High wave-number component T'_w at $AoA = 10°$ (top) overlapped with the τ_w lines (bottom left and right). The straight behavior of $\mathfrak{S}$ observed in Fig. 2(a) is smeared by the presence of two weak disturbances, one close to the saddle point (detail at left bottom) and one at the isotropic node (detail at right, bottom).

Acknowledgements

This work has been supported by the Flagship Project RITMARE, The Italian Research for the Sea, coordinated by the Italian National Research Council and funded by the Italian Ministry of Education, University and Research. Carsten Fuchs (DLR) is acknowledged for TSP surface treatment.

References

Burgmann S and Schröder W (2008) Investigation of the vortex induced unsteadiness of a separation bubble via time-resolved and scanning PIV measurements. *Experiments in Fluids* 45:675–691

Capone A, Klein C, Di Felice F, Beifuss U, and Miozzi M (2015) Fast-response underwater TSP investigation of subcritical instabilities of a cylinder in crossflow. *Experiments in Fluids* 56:1–14

Délery J (2013) *Three-dimensional separated flows topology: Singular points, beam splitters and vortex structures*. pages 1–155

Fey U, Engler R, Egami Y, Iijima Y, Asai K, Jansen U, and Quest J (2003) Transition detection by temperature sensitive paint at cryogenic temperatures in the european transonic wind tunnel (etw). in *ICIASF Record, International Congress on Instrumentation in Aerospace Simulation Facilities*. pages 77–88

Liu T and Sullivan JP (2005) *Pressure-and Temperature-Sensitive Paints*. Wiley Online Library

Liu T and Woodiga S (2011) Feasibility of global skin friction diagnostics using temperature sensitive paint. *Measurement Science and Technology* 22:115402

Miozzi M, Capone A, Costantini M, Fratto L, Klein C, and Di Felice F (2018) Skin friction and coherent structures within a laminar separation bubble. Submitted to Experiments in Fluids

Miozzi M, Capone A, Di Felice F, Klein C, and Liu T (2016) Global and local skin friction diagnostics from TSP surface patterns on an underwater cylinder in crossflow. *Physics of Fluids* 28:124101

Ondrus V, Meier R, Klein C, Henne U, Schäferling M, and Beifuss U (2015) Europium 1,3-di(thienyl)propane-1,3-diones with outstanding properties for temperature sensing. *Sensors and Actuators A: Physical* 233:434 – 441

Schafer RW (2011) What is a Savitzky-Golay filter?. *IEEE Signal Processing Magazine* 28:111–117

Surana A, Grunberg O, and Haller G (2006) Exact theory of three-dimensional flow separation. Part 1. Steady separation. *Journal of fluid mechanics* 564:57–103

Tropea C, Yarin AL, and Foss JF (2007) *Springer handbook of experimental fluid mechanics*. volume 1. Springer Science & Business Media